

Multiwavelength-Integrated Local Model Fitting Method for Interferometric Surface Profiling

Akihiro Yamashita

Tokyo Institute of Technology

2-12-1 O-okayama, Meguro-ku, Tokyo, 152-8552, Japan

yamashita@sg.cs.titech.ac.jp

Masashi Sugiyama

Tokyo Institute of Technology

2-12-1 O-okayama, Meguro-ku, Tokyo, 152-8552, Japan

sugi@cs.titech.ac.jp

Katsuichi Kitagawa

Toray Engineering Co., Ltd.

1-1-45 Oe, Otsu, Shiga, 520-2141, Japan

katsuichi_kitagawa@toray-eng.co.jp

Hisashi Kobayashi

Toray Engineering Co., Ltd.

1-1-45 Oe, Otsu, Shiga, 520-2141, Japan

hisashi_kobayashi@toray-eng.co.jp

Abstract

The *local model fitting* (LMF) method is a useful single-shot surface profiling algorithm that features fast measurement speed and robustness against vibration. However, the measurement range of the LMF method (i.e., measurable height difference between two neighboring pixels) is limited up to a quarter of the light source wavelength. To cope with this problem, the *multiwavelength-matched LMF* (MM-LMF) method was proposed, where the plain LMF method is first applied individually to interference images obtained from multiple light sources with different wavelengths, and then the LMF solutions are matched to obtain a range-extended solution. Although the MM-LMF method was shown to provide high measurement accuracy under moderate noise, phase unwrapping errors can occur if individual LMF solutions are erroneous. In this paper, we propose the *multiwavelength-integrated LMF* (MI-LMF) method that directly computes a range-extended solution from multiple interference images in an integrated way. The effectiveness of the proposed MI-LMF method is demonstrated through simulations and actual experiments.

1 Introduction

Interferometric surface profiling allows an accurate, fast, and non-destructive measurement of nano-scale objects. For this reason, it is used for quality control of various industrial products such as semi-conductors and display panels [1].

The *phase-shift method* [2] is a classic interferometric surface profiling method that uses multiple interference images taken by changing the relative distance between the target object and the reference mirror. Although the phase-shift method provides high measurement accuracy, it is vulnerable to disturbance such as vibration.

To overcome this weakness, single-shot surface profiling methods have been developed. The single-shot methods use only a single interference image that has spatial fringe patterns introduced by tilting the reference mirror. Several algorithms for single-shot surface profiling have been proposed: The *Fourier transform method* [3], the *spatial phase detection method* [4], the *spatial phase synchronization method* [5], the *windowed Fourier transform method* [6], the *spatial phase-shift method* [7, 8], and the *local model fitting (LMF) method* [9]. Among these single-shot methods, the LMF method was shown to be particularly useful.

The measurement principle of the LMF method relies on the assumption that the target surface to be profiled is *locally* flat. This assumption enables us to utilize the information brought by nearby pixels in the single interference image for robust local model fitting. The locality of LMF allows the measurement of objects with sharp steps and/or covered with heterogeneous materials, which is an advantage over the Fourier transform method and the spatial-phase synchronization method. The windowed Fourier transform method also processes the fringe image locally, but it requires the assumption that the target surface to be profiled is sufficiently smooth. The spatial phase-shift method does not suffer from this problem, but it requires the reference mirror to be exactly tilted to a specified angle, which is hard to achieve in practice. The spatial phase detection method does not suffer from this problem, but its height estimation is performed only from a number of pixels on a line segment with width corresponding to a single wavelength. Thus, under a noisy environment, the spatial phase detection method tends to be inaccurate. The LMF method can be regarded as an extension of the spatial phase detection method in that *any* pixels in the vicinity of the target pixel can be used for height estimation, as long as the local flatness is not strongly violated.

However, in the original LMF method, the measurement range (i.e., measurable height difference between two neighboring pixels) is limited up to a quarter of the light source wavelength. To extend the measurement range, the *multiwavelength-matched LMF (MM-LMF) method* [10] was proposed. The MM-LMF method uses multiple interference images generated by multiple light sources with different wavelengths. In the MM-LMF method, a range-extended solution is obtained by a two-stage process: The plain LMF method is first applied individually to multiple interference images, and then a range-extended solution is computed from the LMF solutions by matching the individual LMF solutions.

Although the MM-LMF method was shown to provide high measurement accuracy under moderate noise, peaky artifacts are often observed in the final measurement result

under noisy environments. Such artifacts typically occur under a high spatial-resolution measurement because the size of local windows in LMF needs to be made small, which reduces the number of samples used for estimation. Consequently, the final measurement result becomes susceptible to noise and this accuracy degradation causes phase-unwrapping errors in the second stage of the MM-LMF method.

To cope with the problem, we propose a new method called the *multiwavelength-integrated LMF (MI-LMF) method*, which computes an estimate of the surface profile from multiple interference images in an integrated way. This highly mitigates the problem of suffering from peaky artifacts caused by phase-unwrapping errors. The effectiveness of the MI-LMF method is demonstrated through computer simulations and actual experiments.

The rest of this paper is structured as follows. In Section 2, we briefly review the LMF and the MM-LMF methods. In Section 3, we describe our proposed method and demonstrate its effectiveness through computer simulations and actual measurement experiments. Finally, we conclude in Section 4.

2 Review of Existing Methods

In this section, we briefly review the measurement principles of the LMF method [9] and the MM-LMF method [10].

2.1 The Local Model Fitting Method

We tilt the reference mirror in an arbitrary angle. Then an interference pattern at (x, y) is given as

$$g(x, y) := a(x, y) + b(x, y) \cos \left(\frac{4\pi z(x, y)}{\lambda} + 2\pi px + 2\pi qy \right), \quad (1)$$

where $a(x, y)$ and $b(x, y)$ are the bias and the amplitude, $z(x, y)$ denotes a relative height of a target object, λ is the wavelength of a light source, and p and q are spatial carrier frequencies along the x - and y -axes, respectively. The goal of the LMF method is to estimate $z(x, y)$ from the observed interference image.

In the LMF method, we consider a local area for each target point (x, y) , and assume that $a(x, y)$, $b(x, y)$, and $z(x, y)$ take constant values a , b , and z in the local area, respectively. Furthermore, because we can estimate p and q in advance using global information of the fringe image such as the number of fringe patterns, we replace them by their estimates \hat{p} and \hat{q} . Then the intensity value at a point (x, y) in the local area is modeled as

$$\bar{g}(x, y) := a + b \cos \left(\frac{4\pi z}{\lambda} + 2\pi \hat{p}x + 2\pi \hat{q}y \right), \quad (2)$$

where unknown parameters in this local model are only a , b , and z .

After having some variable transformations, $\bar{g}(x, y)$ can be rewritten as

$$\bar{g}(x, y) = a + \xi\varphi(x, y) + \zeta\psi(x, y), \quad (3)$$

where

$$\xi := b \cos\left(\frac{4\pi z}{\lambda}\right), \quad (4)$$

$$\zeta := b \sin\left(\frac{4\pi z}{\lambda}\right), \quad (5)$$

$$\varphi(x, y) := \cos(2\pi\hat{p}x + 2\pi\hat{q}y), \quad (6)$$

$$\psi(x, y) := -\sin(2\pi\hat{p}x + 2\pi\hat{q}y). \quad (7)$$

Unknown parameters in Eq. (3) are a , ξ , and ζ . To determine these parameters, this local model is fitted to observed intensity values $\{g_i\}_{i=1}^n$ in the vicinity of the target point by least-squares:

$$(\hat{a}, \hat{\xi}, \hat{\zeta}) := \underset{(a, \xi, \zeta)}{\operatorname{argmin}} \sum_{i=1}^n (g_i - \bar{g}(x_i, y_i))^2. \quad (8)$$

Because the local model is linear with respect to a , ξ , and ζ , the least-squares solutions \hat{a} , $\hat{\xi}$, and $\hat{\zeta}$ can be analytically obtained as

$$(\hat{a}, \hat{\xi}, \hat{\zeta})^\top = (\mathbf{A}^\top \mathbf{A})^{-1} \mathbf{A}^\top \mathbf{g}, \quad (9)$$

where $^\top$ denotes the transpose, and \mathbf{A} is the $n \times 3$ matrix and \mathbf{g} is the n -dimensional vector defined by

$$\mathbf{A} := \begin{pmatrix} 1 & \varphi(x_1, y_1) & \psi(x_1, y_1) \\ \vdots & \vdots & \vdots \\ 1 & \varphi(x_n, y_n) & \psi(x_n, y_n) \end{pmatrix} \quad \text{and} \quad \mathbf{g} := \begin{pmatrix} g_1 \\ \vdots \\ g_n \end{pmatrix}. \quad (10)$$

We can estimate *candidates* of the target height using $\hat{\xi}$ and $\hat{\zeta}$ as

$$\hat{z}(k) := \frac{\lambda}{4\pi} \arctan\left(\frac{\hat{\xi}}{\hat{\zeta}}\right) + \frac{\lambda k}{2}, \quad (11)$$

where k is an unknown integer called the order of interference. k can be determined by a proper phase-unwrapping algorithm [11], if the height difference between two neighboring pixels is less than a quarter of the wavelength.

Note that an estimate of the amplitude \hat{b} can also be obtained using $\hat{\xi}$ and $\hat{\zeta}$ as

$$\hat{b} = \sqrt{\hat{\xi}^2 + \hat{\zeta}^2}. \quad (12)$$

2.2 The Multiwavelength-Matched LMF Method

The measurement range of the LMF method is limited up to a quarter of the light source wavelength. To extend the measurement range, the MM-LMF method was proposed [10].

Suppose we observe multiple interference images for light sources with different wavelengths. Let us denote the intensity value of the j -th image at point (x, y) by $g_j(x, y)$ ($j = 1, \dots, m$). Then $g_j(x, y)$ is modeled as

$$g_j(x, y) := a_j(x, y) + b_j(x, y) \cos \left(\frac{4\pi z(x, y)}{\lambda_j} + 2\pi p_j x + 2\pi q_j y \right), \quad (13)$$

where $a_j(x, y)$ and $b_j(x, y)$ are the bias and the amplitude of the fringe pattern, λ_j is the wavelength of the light source, p_j and q_j are spatial carrier frequencies along the x -axis and y -axis, respectively. $z(x, y)$ is the height of the target object, which is common to all $j = 1, \dots, m$. The goal of the MM-LMF method is to estimate a surface profile in an extended range from these multiple interference images.

In the MM-LMF method, the plain LMF method is first applied to each interference image to obtain a set of height candidates. According to Eq. (11), the height candidates $\{\widehat{z}_j(k_j)\}_{j=1}^m$ obtained by the LMF method are written as

$$\widehat{z}_j(k_j) := \frac{\lambda_j}{4\pi} \arctan \left(\frac{\widehat{\xi}_j}{\widehat{\zeta}_j} \right) + \frac{\lambda_j k_j}{2}, \quad (14)$$

where $\{k_j\}_{j=1}^m$ are the orders of interference.

Then the orders $\{k_j\}_{j=1}^m$ are determined so that the following matching error of $\{\widehat{z}_j(k_j)\}_{j=1}^m$ is minimized:

$$(\widehat{k}_1, \dots, \widehat{k}_m) := \underset{(k_1, \dots, k_m)}{\operatorname{argmin}} \left(\max(\widehat{z}_1(k_1), \dots, \widehat{z}_m(k_m)) - \min(\widehat{z}_1(k_1), \dots, \widehat{z}_m(k_m)) \right). \quad (15)$$

Finally, we obtain a range-extended estimate \widehat{z} as

$$\widehat{z} := \frac{1}{m} \sum_{j=1}^m \widehat{z}_j(\widehat{k}_j). \quad (16)$$

3 Proposed Method

In this section, we propose a new single-shot algorithm called the *multiwavelength-integrated LMF (MI-LMF) method*. We first describe an algorithm of the MI-LMF method in a range-unextended measurement in Section 3.1. Then we show how this can be extended to a range-extended measurement in Section 3.2. Finally, we report the results of actual experiments.

3.1 The Multiwavelength-Integrated LMF Method

To estimate a surface profile with a high spatial resolution by the LMF method, the local area needs to be made sufficiently small. However, this causes the number of samples for model fitting to be reduced, and thus the measurement is susceptible to noise in an observed interference image.

Let us illustrate this by computer simulations. Fig. 1(a) shows the surface profile of an artificial object we use here. The surface contains 9 spiky bumps that have 100nm height with 3×3 pixel width. Fig. 1(b) shows multiple interference images generated based on the model (13), and Fig. 1(c) illustrates its one-dimensional plot at $y = 50$. It consists of three interference images for three colors (wavelengths): blue (470nm), green (560nm), and red (600nm). Gaussian noise with mean 0 and standard deviation 10 is added to the intensity value of each pixel in each image. Note that measurement of such spiky bumps under a noisy environment is a highly challenging task.

Because the plain LMF method uses a single interference image, we focus on the image corresponding to blue. Fig. 1(d), (e), and (f) illustrate the results of the LMF method with vicinity sizes 3×3 , 5×5 , and 7×7 , respectively, and Fig. 1(g), (h), and (i) illustrate their one-dimensional plots at $y = 50$. We also included the root mean square error (RMSE) of estimated heights in Fig. 1(d), (e), and (f). When the vicinity size is 5×5 and 7×7 , the bumps tend to be lost due to low spatial resolutions. On the other hand, when the vicinity size is 3×3 , the height of the bumps can be somehow recovered. However, the measurement result is highly degraded by noise.

If we use multiple interference images, the number of samples can be essentially increased even with the same vicinity size. The key idea of the proposed method is to perform model fitting to multiple interference images *simultaneously*.

Let us assume that the height $z(x, y)$ is a constant value z in the local area. We further assume that the bias $a_j(x, y)$ and amplitude $b_j(x, y)$ in the local area have been estimated as $\hat{a}_j(x, y)$ and $\hat{b}_j(x, y)$ by some method¹. Then the local model of the MI-LMF method is given by

$$\bar{g}_j(x, y) := \hat{a}_j(x, y) + \hat{b}_j(x, y) \cos \left(\frac{4\pi z}{\lambda_j} + 2\pi \hat{p}_j x + 2\pi \hat{q}_j y \right), \quad (17)$$

where \hat{p}_j and \hat{q}_j are estimates of p_j and q_j , respectively. Note that an unknown parameter in this model is only z . We estimate it by least-squares model fitting using data points taken from multiple images:

$$\hat{z} := \underset{z}{\operatorname{argmin}} J(z), \quad (18)$$

¹In this paper, we use the following method: We first apply the plain LMF method to each interference image and obtain estimates of the bias $a_j(x, y)$ and amplitude $b_j(x, y)$. Then we apply a 7×7 -pixel median filter to the entire images of $a_j(x, y)$ and $b_j(x, y)$ and use the obtained values as $\hat{a}_j(x, y)$ and $\hat{b}_j(x, y)$.

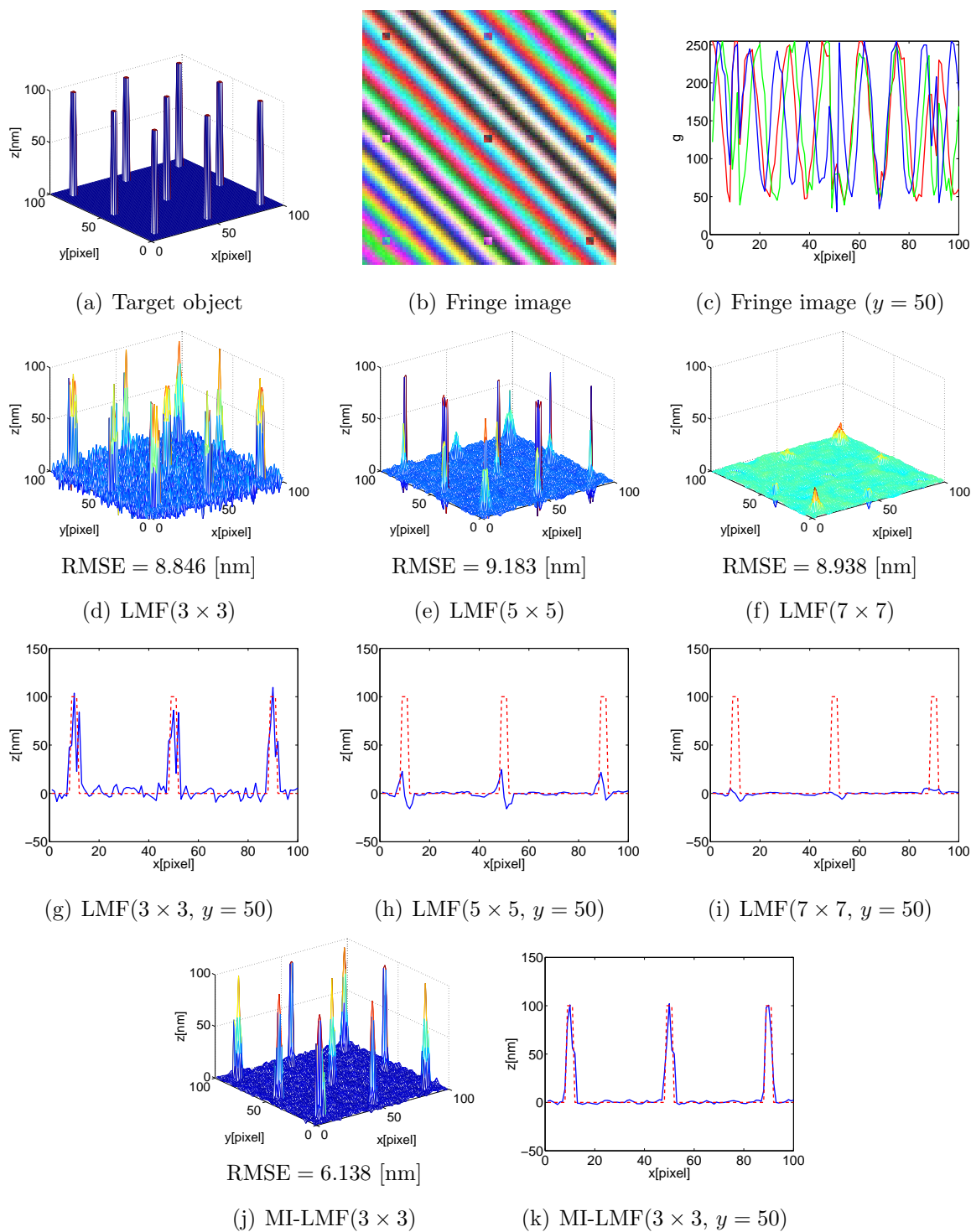


Figure 1: Simulations for spiky bumps.

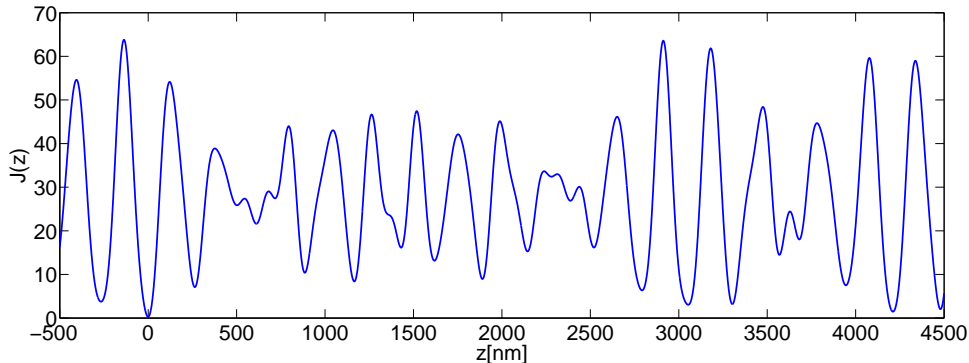


Figure 2: Profile of the error criterion $J(z)$ defined by Eq. (19) at point (25, 25) for the interference image shown in Fig. 1(b). Note that the horizontal axis of this graph corresponds to the vertical axis (i.e., the height) in Fig. 1 and Fig. 3.

where

$$J(z) := \sum_{j=1}^m \frac{1}{c_j} \sum_{i=1}^n (g_{i,j} - \bar{g}_j(x_i, y_i))^2 \quad (19)$$

is an error criterion, $\{g_{i,j}\}_{i=1,j=1}^{n,m}$ are observed intensity values, and $\{c_j\}_{j=1}^m$ are normalization constants for each wavelength:

$$c_j := \frac{1}{n} \sum_{i=1}^n \hat{b}_j(x_i, y_i)^2. \quad (20)$$

If the amplitude of fringe patterns differs in multiple wavelengths, an image with a larger amplitude will dominate the error criterion (19). To prevent this, the above normalization constants were introduced.

Fig. 2 illustrates the error function $J(z)$ defined by Eq. (19) at point (25, 25) in the interference image shown in Fig. 1(b). Note that the true height at (25, 25) is zero. As the graph shows, $J(z)$ actually has many local minima. Here, we use a *gradient-descent method* with the initial point set at the solution of the LMF method obtained from the blue image.

Finally, we report simulation results. Fig. 1(j) illustrates the result of the MI-LMF method for the interference images shown in Fig. 1(b), and Fig. 1(k) illustrates its one-dimensional plot at $y = 50$. The vicinity size is set to 3×3 . We can see that the bumps are restored clearly with less noise.

3.2 Range-Extension of the MI-LMF Method

The MM-LMF method takes a two-stage process to obtain a range-extended solution from multiple interference images. In the first stage, the plain LMF method is applied to each image individually to obtain height candidates. Then, in the second stage, the LMF

solutions are matched to determine the order of interference. If larger errors are incurred in individual measurement results, order matching fails and thus peaky artifacts appear in the final measurement result.

Let us illustrate this by computer simulations. Fig. 3(a) illustrates the surface profile of an artificial object. The surface has 9 *super*-spiky bumps, which are similar to the spiky bumps in Fig. 1(a). However, the height of bumps in Fig. 3(a) is 4000nm, which is 40 times higher than that in Fig. 1(a). Fig. 3(b) shows multiple interference images generated in the same way as Section 3.1, and Fig. 3(c) illustrates its one-dimensional plot at $y = 50$.

Fig. 3(d), (e), and (f) show the measurement results obtained by the MM-LMF method with vicinity sizes 3×3 , 5×5 , and 7×7 , respectively, and Fig. 3(h), (i), and (j) illustrate their one-dimensional plots at $y = 50$. As shown in these graphs, a small vicinity size such as 3×3 is required to accurately measure the height of the bumps. However, this causes high susceptibility to noise.

To obtain a range-extended solution by the MI-LMF method, we use the gradient-descent method with multiple initial points. More precisely, we first apply the plain LMF method to one of the interference images and obtain height candidates $\{\hat{z}_1(k_1)\}_{k_1}$ in some range. Then we run the gradient-descent method with $\{\hat{z}_1(k_1)\}_{k_1}$ as initial values and find a set of local minima $\{\hat{z}_{k_1}\}_{k_1}$. Finally, from $\{\hat{z}_{k_1}\}_{k_1}$, we choose the solution \hat{z} that minimizes the error criterion (19).

Now, we report simulation results of the above algorithm. Fig. 3(j) illustrates an estimated surface profile obtained by the extend range algorithm, and Fig. 3(k) illustrates its one-dimensional plot at $y = 50$. We can see that spiky artifacts are suppressed and the profile of bumps is clearly restored.

3.3 Actual Measurement Experiments

Finally, we report the results of actual experiments. We obtained multiple interference images by the multiwavelength single-shot surface profiler *MW-500* developed by Toray Engineering Co., Ltd² (see Fig. 4(a)). The target object to measure is a color filter for a flat-panel display.

Fig. 4(b) shows a simplified diagram of the structure of our surface profiler, which consists of 3 light sources, a color camera, a beam splitter, and a reference mirror. Three-wavelength composite light given off from the light sources is separated into two different directions by the beam splitter: One goes down to the target object and the other goes to the reference mirror. The reflected lights are recombined at the beam splitter and then taken by the camera. The reference mirror are tilted so that spatial fringe patterns are introduced. A notable feature of this measurement system is that, thanks to the combination of a three-color light source and a color camera, single-shot measurement of 3 interference images is possible.

Fig. 4(c) shows the obtained fringe image, which consists of 3 interference images with different wavelengths: 471nm (blue), 559nm (green), and 600nm (red). The size of a pixel

²See '<http://www.scn.tv/user/torayins/>' for details.

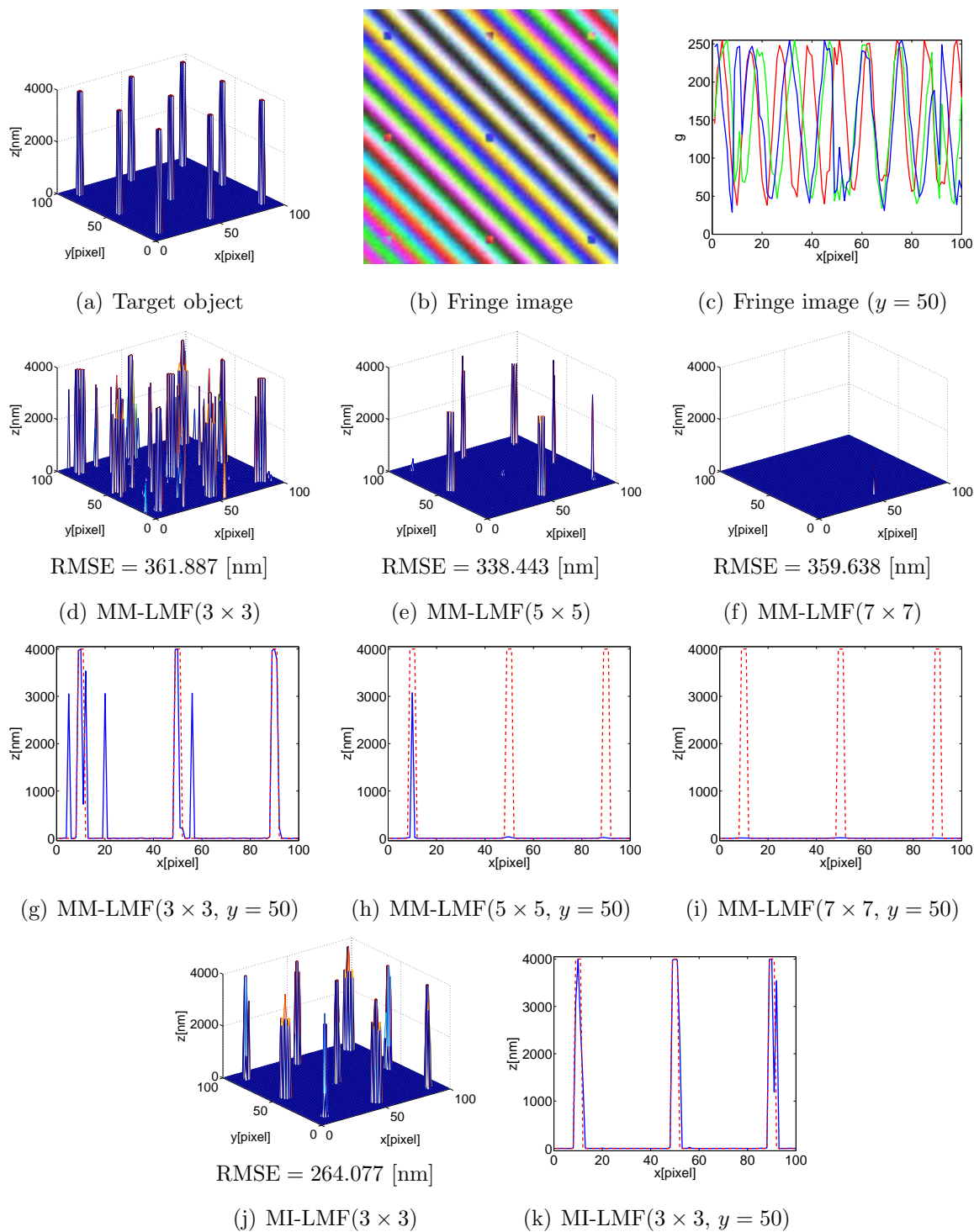
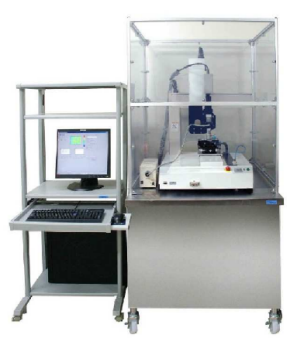
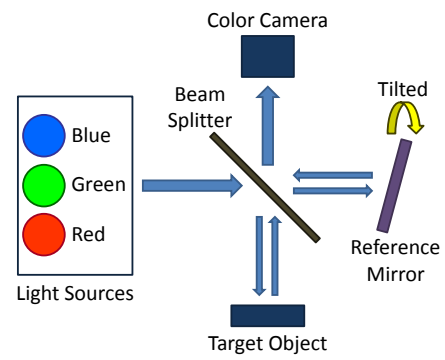


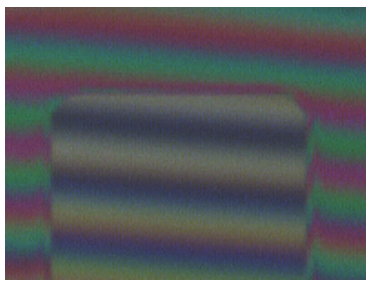
Figure 3: Simulations for super-spiky bumps.



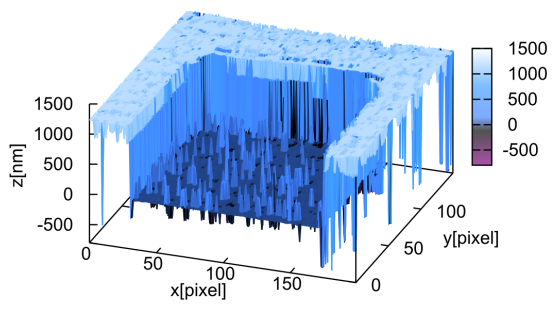
(a) MW-500



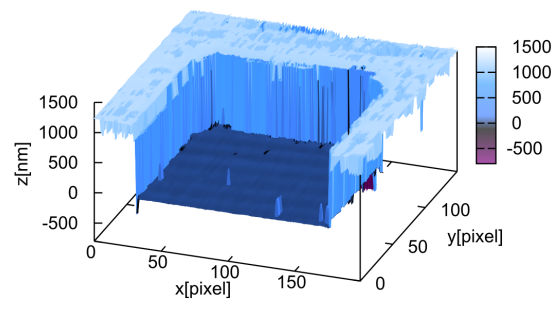
(b) Simplified diagram of MW-500



(c) Fringe image



(d) Result of MM-LMF



(e) Result of MI-LMF

Figure 4: Actual measurement results.

in the image is $1.28\mu\text{m}$ by $1.28\mu\text{m}$. We applied the MM-LMF method and the MI-LMF method to these interference images, and estimated the surface profile. The vicinity size was set to 13 (vertical) \times 3 (horizontal) pixels³.

Fig. 4(d) and Fig. 4(e) show surface profiles estimated by the MM-LMF method and the MI-LMF method, respectively. We can see that large spiky artifacts are incurred in the MM-LMF result, whereas such artifacts are substantially reduced in the MI-LMF result.

4 Conclusion

The MM-LMF method has useful characteristics such as fast measurement speed, robustness against vibration, and a measurement range over a quarter of the light source wavelength. However, the MM-LMF method tends to suffer from phase unwrapping errors particularly when the spatial resolution of the LMF method is set to be high. In this paper, we proposed a new multiwavelength single-shot surface profiling algorithm called the MI-LMF method, which directly estimates the surface profile from multiple interference images in an integrated way. The usefulness of the proposed method was demonstrated by computer simulations and actual measurement experiments.

References

- [1] S. W. Kim, “High-speed 3d inspection for densely packed semiconductor chips,” <http://spie.org/x24235.xml?ArticleID=x24235>.
- [2] J. H. Brunning, D. R. Herriott, J. E. Gallagher, D. P. Rosenfeld, A. D. White, and D. J. Brangaccio, “Digital wave front measuring interferometer for testing optical surface and lenses,” *Applied Optics* **13**, 2693–2703 (1974).
- [3] M. Takeda, H. Ina, and S. Kobayashi, “Fourier-transform method of fringe-pattern analysis for computer-based topography and interferometry,” *Journal of Optical Society of America* **72**, 156–160 (1982).
- [4] S. Toyooka and Y. Iwaasa, “Automatic profilometry of 3-d diffuse objects by spatial phase detection,” *Applied Optics* **25**, 1630–1633 (1986).
- [5] J. Kato, I. Yamaguchi, T. Nakamura, and S. Kuwashima, “Video-rate fringe analyzer based on phase-shifting electronic moiré patterns,” *Applied Optics* **36**, 8403–8412 (1997).

³In this experiment, we were interested in the sharpness of the steps along the x -axis. A practical heuristic for accurate measurement is to introduce a spatial carrier orthogonal to the direction of interest, i.e., along the y -axis. Following this heuristic, we decided to use a rectangular-shaped local area along the y -axis.

- [6] Q. Kemao, “Windowed Fourier transform for fringe pattern analysis,” *Applied Optics* **43**(13), 2695–2702 (2004).
- [7] D. C. Williams, N. S. Nassar, J. E. Banyard, and M. S. Virdee, “Digital phase-step interferometry: A simplified approach,” *Optics & Laser Technology* **23**, 147–150 (1991).
- [8] N. Brock, J. Hayes, B. Kimbrough, J. Millerd, M. North-Morris, M. Novak, and J. C. Wyant, “Dynamic interferometry,” in “Novel Optical Systems Design and Optimization VIII, Proceedings of SPIE,” , vol. 5875, J. M. Sasián, R. J. Koshel, and R. C. Juergens, eds. (2005), vol. 5875, pp. 1–10.
- [9] M. Sugiyama, H. Ogawa, K. Kitagawa, and K. Suzuki, “Single-shot surface profiling by local model fitting,” *Applied Optics* **45**, 7999–8005 (2006).
- [10] K. Kitagawa, “Fast surface profiling by multi-wavelength single-shot interferometry,” *International Journal of Optomechatronics* **4**, 136–156 (2010).
- [11] M. Takeda and T. Abe, “Phase unwrapping by a maximum cross-amplitude spanning tree algorithm: A comparative study,” *Optical Engineering* **35**, 2345–2351 (1996).